Available online at www.sciencedirect.com
ScienceDirect
Journal of Nuclear Materials 372 (2008) 76–88
journal of nuclear materials
www.elsevier.com/locate/jnucmat

Creep in phosphorus alloyed copper during power-law breakdown

Rolf Sandström [a,b,*], Henrik C.M. Andersson [b]

[a] Materials Science and Engineering, Royal Institute of Technology, Brinellvägen 23, S-10044 Stockholm, Sweden
[b] Corrosion and Metals Research Institute, Drottning Kristinas väg 48, S-11428 Stockholm, Sweden

Received 30 January 2007; accepted 23 February 2007

Abstract

During the first phase of storage, creep will take place in the copper canisters in the KBS-3 package for nuclear waste. The temperatures are below 100 °C, and the creep is well inside the power-law breakdown regime. Creep models for this situation have been developed. The analysed material is pure copper with about 50 ppm phosphorus. Constitutive equations for creep and other plastic deformation have been set up based on a generalised Norton expression and Kocks–Mecking's model for the back stress. A model for the minimum creep rate based on fundamental principles for climb and glide has been derived. This model gives the correct order of magnitude for the creep rate in the temperature range from 400 to 20 °C without the use of fitted parameters. The creep exponent varies from 5 to 105 in this interval. The constitutive equations have also been formulated for multiaxial stress states.

PACS: 83.10.Gr; 81.70.Bt; 87.15.La

1. Introduction

According to the proposed method in Sweden the nuclear waste will be placed in a package consisting of a cast iron insert and an outer 50 mm thick copper vessel [1]. The waste packages are to be placed in a depository 500 m below ground. Copper was selected because it is immune against corrosion under reducing conditions in the bedrock. Creep in the waste package is expected to take place when the surrounding bentonite clay absorbs water, which gives rise to a swelling pressure. Due to creep in the copper, the existing gap between the canister and the cast iron insert is gradually closed. The waste package is designed to ensure that the temperature does not exceed 100 °C. Creep may also occur if the canister is sheared during an earthquake. The temperature in such a case would be close to ambient.

To avoid problems with low creep ductility in high purity oxygen-free high conductivity (Cu-OF) copper [2], copper with additions of about 50 ppm phosphorus (Cu-OFP) is now considered [3]. Even in the low temperature range of interest for the waste package of 0–100 °C, creep is taking place [4]. There is a dramatic change in the creep behaviour of copper in the interval 175–300 °C [2]. In particular, there is a large increase in the creep exponent, which is traditionally referred to as power-law breakdown. In many papers it is proposed that the stress dependence can be described by a factor of the form $\exp(\beta\sigma)$ where β is a constant and σ the applied stress. However, this form does not give an adequate representation for copper.

The purpose of the present paper is to develop a fundamental model that can describe the stress and temperature of the creep rate for Cu-OFP. In addition constitutive equations for plastic deformation and creep in copper are presented. The focus will be on the power-law breakdown regime (<300 °C).

2. Material data

The traditional way of determining creep properties is to perform creep strain or rupture tests with dead weight

* Corresponding author. Address: Materials Science and Engineering, Royal Institute of Technology, Brinellvägen 23, S-10044 Stockholm, Sweden. Fax: +46 8 203107.
E-mail address: rsand@kth.se (R. Sandström).

0022-3115/$ - see front matter © 2007 Published by Elsevier B.V.
doi:10.1016/j.jnucmat.2007.02.005

loading. For the type of P-doped copper that is intended for copper canisters, many such tests have been performed [5–10]. They will be utilised in the present assessment. In addition results from slow rate tensile tests will be used [4]. This testing technique has several advantages. It avoids the large initial plastic strain of 5–15% in the creep tests. In addition it somewhat simulates the situation in the canisters, when the initial loading is established. Creep testing on the other hand has the advantage that equipment is readily available for performing long term tests.

The batches considered are listed in Table 1. Their impurity content, their grain size and the mechanical properties are summarised. Only one batch has been considered for slow strain rate tensile tests (SSR), namely the last one. This is the only batch that has been cold worked, since it is taken from a rolled formed canister. The amount of cold work in the processing has been estimated to 8%. All the other batches have been used for creep testing.

The amount of testing for each batch is listed in Table 2. The test temperatures are given together with the number of tests at each temperature (in brackets). Most of the batches have a phosphorus content between 50 and 70 ppm. One batch has a higher content and one a lower one. The four batches tested at 175 °C have been found to have quite similar creep properties independently of phosphorus content and grain size. They are handled as one set in the present assessment.

3. Constitutive model

3.1. Basic assumptions

The total strain rate ε_{tot} is considered to consist of the elastic strain rate and the creep strain rate

$$\frac{d\varepsilon_{tot}}{dt} = \frac{1}{E}\frac{d\sigma}{dt} + A\sigma_{eff}^{n}, \quad (1)$$

where E is the elastic modulus, t the time, and σ the stress. A and n are constants. The effective stress σ_{eff} is the difference between the applied stress σ and an internal back stress σ_i

$$\sigma_{eff} = \sigma - \sigma_i. \quad (2)$$

The internal stress can be defined and modelled in different ways. It cannot be measured in an unambiguous way. It should therefore be considered as a model quantity. In our case the internal stress is assumed to be the result of work hardening in the material.

The dislocation generation during plastic deformation is often expressed as

$$\frac{d\rho}{d\varepsilon} = \frac{m}{bL} - 2\omega\rho, \quad (3)$$

where ρ is the dislocation density, ε the plastic strain, m the Taylor factor, b Burgers vector, L the mean free path of released dislocations, and ω a constant. The first term on the

Table 1
Characteristics of analysed materials

Material number	Test series	Grain size (μm)	P (ppm)	S (ppm)	H (ppm)	O (ppm)	Yield strength $R_{p0.2}$ (MPa)	Tensile strength R_m (MPa)	Elongation (%)	Reduction in area Z (%)	Hardness (*HV*)
2	CuP30_450	450	29	6	<0.5	1.2	–	–	–		53
3	CuP60_350	350	58	6	<0.5	1.1	52	225	45		55
4	CuP105_450	450	106	5	<0.5	1.1	51	224	46		–
6	CuP60_100	100	58	6	<0.5	–	56	231	46		55
400[a]	Cu-OFP400	45	50	6	<0.10	0.90	46	239	60		40
400[a]	Cu-OFP400		59				97	243	46	94	54
500	Cu-OFP500		54				93	202	42	76	53
900	Cu-OFP SSR		50[b]				209	226			116

[a] Two assessments have been performed.
[b] Estimated value.

Table 2
Creep and slow strain rate tests included in the assessment

Material number	Test series	Test temperatures and number of specimens (°C)	Comment	Reference
2	CuP30_450	175 (4)		[9]
3	CuP60_350	175 (5)		[9]
4	CuP105_450	175 (4)		[9]
6	CuP60_100	175 (4)		[9]
400	Cu-OFP400	215 (5), 250 (3), 300 (4), 350 (2), 400 (2), 450 (1)		[5,7]
500	Cu-OFP500	200 (1), 215 (3), 250 (3), 275 (3), 300 (3), 325 (1), 350 (2)		[5–7]
900	Cu-OFP SSR	20 (2), 75 (4), 125 (4), 175 (4)	Slow strain rate tensile testing; cold worked material	[4]

right hand side represents the work hardening and the second term the dynamic recovery. Following Kocks and Mecking [11], L is assumed to be proportional to $1/\sqrt{\rho}$ which means that the dislocation movement is controlled by the forest of other dislocations. The back stress is related to the dislocation density

$$\sigma_i = \sigma_{i0} + \alpha G b \sqrt{\rho}, \tag{4}$$

where G is the shear modulus, σ_{i0} and α are constants. Due the assumptions above, σ_{i0} vanishes in our case. If (4) is inserted into (3), the following relation is obtained:

$$\frac{d\sigma_i}{d\varepsilon} = \omega(C - \sigma_i), \tag{5}$$

where C is a constant that can be expressed in the other constants in Eqs. (3) and (4). Eq. (5) can be integrated directly if ω and C are constants

$$\sigma_i = C - C_1 e^{-\omega\varepsilon}, \tag{6}$$

where C_1 is a constant that is found from the initial value of σ_i. Since σ_i is assumed to represent the work hardening, $\sigma_i = 0$ for $\varepsilon = 0$. This gives $C_1 = C$. Eqs. (5) and (6) are referred to as the Kocks–Mecking model for plastic deformation. This model has often turned out to give a good description of plastic deformation of fcc alloys. Eq. (1) together with (5) or (6) represent a model for describing the plastic deformation of materials including creep. Next the constants in Eq. (1) will be determined by comparison to creep and slow strain rate tensile tests.

3.2. Stationary creep

The minimum (stationary) creep rate of many alloys can be described by the following equation:

$$\left.\frac{d\varepsilon_{cr}}{dt}\right|_{min} = A\sigma^n e^{\beta\sigma} e^{-\frac{q}{RT}}, \tag{7}$$

where ε_{cr} is the creep strain, t the time, $\left.\frac{d\varepsilon_{cr}}{dt}\right|_{min}$ is the minimum creep rate, σ the applied stress, and T the absolute temperature. A, n, β, and q are constants, and R the gas constant. Eq. (7) can be derived from fundamental facts in physical metallurgy if the creep is assumed to be controlled by climb of dislocations. Since a wide temperature range of copper data will be considered, Eq. (7) is not sufficient in its basic form. Above a characteristic temperature for each material, the creep exponent n is 4–6. This is referred to as power-law creep. Below this temperature and at high stresses the creep exponent becomes much larger. This is called power-law breakdown. Although the factor $e^{\beta\sigma}$ in Eq. (7) gives an increase in the creep exponent with increasing stress, the effect is not large enough. For that reason the following generalised form of Eq. (7) will be used:

$$\left.\frac{d\varepsilon_{cr}}{dt}\right|_{min} = A\sigma^{n(T)} e^{\beta(\sigma)} e^{-\frac{q(T)}{RT}}. \tag{8}$$

In Eq. (8), $n(T)$ and $q(T)$ are assumed to be functions of T, and $\beta(\sigma)$ a function of σ. For the creep tests the minimum creep rate and the applied stress σ are utilised in Eq. (8). For the tensile tests, the stationary situation is considered. The creep rate is then the total strain rate and the stationary engineering stress the σ value. The physical basis of Eq. (8) will be discussed in Section 4. For data in the temperature intervals 20–175 °C and 200–400 °C, the fit is illustrated in Fig. 1.

For the creep data the minimum creep rate is given versus stress in Fig. 1. For the slow strain rate tests, the strain rate versus the stationary stress is shown. A second order polynomial has been used for $\beta(\sigma)$. For $q(T)$ the form $q(T) = -RT\gamma(T_C)$ has been assumed where $\gamma(T_C)$ is a second order polynomial in the Celsius temperature T_C. The reason for keeping T_C instead of the absolute temperature in the expression for $q(T)$ is to avoid numerical difficulties that otherwise easily appear due to the presence of very large numbers. The fit to data is in general acceptable except possibly at 175 °C. At this temperature the slow strain rate tensile tests (SSR) show a higher strain rate than the creep tests. The reason for this difference will be discussed below. The parameter values used in Eq. (8) are given in Table 3.

An effective creep exponent N can be defined from Eq. (8)

$$N = \left.\frac{\partial \log \dot{\varepsilon}_{cr}}{\partial \log \sigma}\right|_{min} = n(T) + \sigma\frac{d\beta(\sigma)}{d\sigma}. \tag{9}$$

The effective creep exponent N as a function of stress and temperature is shown in Fig. 2.

The creep exponent increases with decreasing temperature from 45 to 60 at 175 °C to 105 at 20 °C. Such high creep exponents have also been observed for steels at 320–360 °C, that is 150 °C below the normal creep range for unalloyed steels [12]. If we limit ourselves to temperatures above 200 °C, the behaviour of the data is different, see Fig. 1. The slope of the curves is much lower, which is also apparent from the creep exponent, see Fig. 2(b). As pointed out above the creep exponent in the power-law regime is 4–6. This takes place for stresses below 60 MPa.

Representations based on Eq. (8) can only be extrapolated to a limited extent outside the experimental data ranges. The maximum application interval is summarised in Table 4.

3.3. Stress–strain curves

With the aid of Eqs. (1), (2) and (5) for the back stress σ_i, the stress–strain curve during a tensile test can be modelled. The creep rate now takes the form

$$\left.\frac{d\varepsilon_{cr}}{dt}\right|_{min} = A\sigma_{eff}^{n(T)} e^{\beta(\sigma_{eff})} e^{-\frac{q(T)}{RT}}. \tag{10}$$

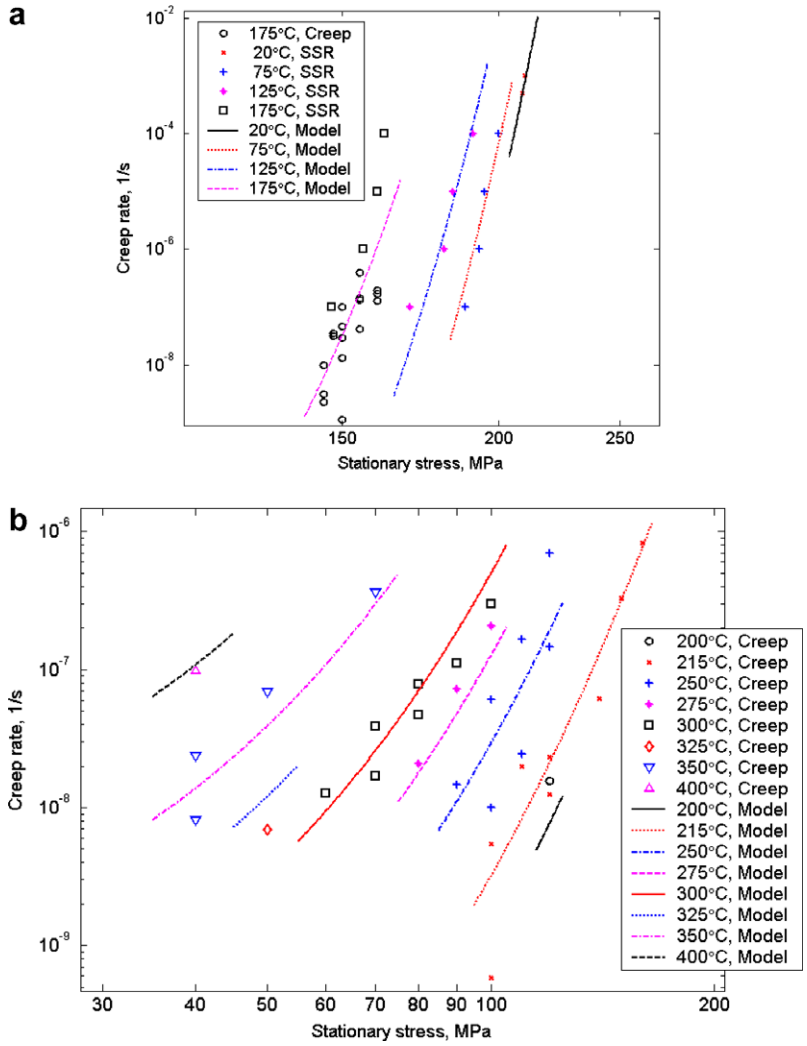

Fig. 1. Creep rate as a function of stress. SSR refers to slow strain rate tensile tests. (a) Data interval 20–175 °C and (b) data interval 200–400 °C.

Table 3
Constants in Eq. (8)

Temperature range (°C)	A (1/s)	n	β_1 (1/MPa)	β_2 (1/MPa^2)	γ_1 (1/°C)	γ_2 (1/°C^2)	Fig. no.
20–175	5.40×10^{-23}	0	-9.08×10^{-2}	14.3×10^{-4}	-0.727×10^{-2}	5.46×10^{-4}	1a
200–400	2.00×10^{-21}	0.00323	11.12×10^{-2}	-0.771×10^{-4}	9.92×10^{-2}	-0.774×10^{-4}	1b
20–175	6.33×10^{11}	0	-90.5×10^{-2}	35.4×10^{-4}	2.12×10^{-2}	6.67×10^{-4}	6

$\beta(\sigma)=\beta_1\sigma+\beta_2\sigma^2;\ \gamma(T_C)=\gamma_1 T_C+\gamma_2 T_C^2$.

Replacing the last term in Eq. (1) by (10) gives

$$\frac{d\sigma}{dt}=E\frac{d\varepsilon_{tot}}{dt}-EA\sigma_{eff}^{n(T)}e^{\beta(\sigma_{eff})}e^{-\frac{q(T)}{RT}}. \quad (11)$$

During a tensile test the total strain rate is constant and Eqs. (5) and (11) can be integrated directly. There are two constants C and ω in Eq. (5). C can be taken as the true tensile strength, which is about 285 MPa at room temperature. At higher temperature, C is reduced in proportion to the temperature dependence of the shear modulus G [13]

$$G=4.75\times10^4-17T,$$

where G is given in MPa and T is the absolute temperature. The following model is assumed for ω [14,15]:

$$\omega=\frac{B\dot{\varepsilon}^{n_b}}{(T-273)^{p_b}}, \quad (12)$$

where B, n_b and p_b are constants that are determined by fitting to the stress–strain curves. The following values were found: $B=4.02$, $n_b=0.0481$, and $p_b=0.277$. The fit is illustrated in Fig. 3.

There is considerable scatter in the experimental values for ω as can be seen from Fig. 3. It is clear that ω increases

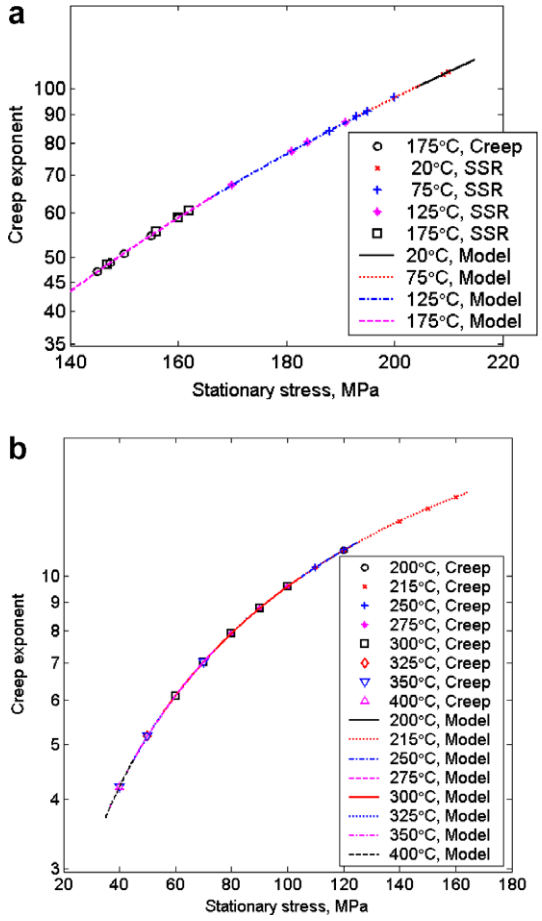

Fig. 2. Effective creep exponent N as a function of stress. (a) Data interval 20–175 °C and (b) data interval 200–400 °C.

with increasing strain rate and decreasing temperature. The use of Eq. (11) is illustrated for two tensile tests in Fig. 4. For strain rates of 0.0001 1/s and below, the engineering stress quickly reaches a stationary value. For the tensile tests performed at 75–175 °C and 1×10^{-4}–1×10^{-7} 1/s the flow curves are at the correct position showing that Eq. (8) can describe the stationary stress. The true stress is also influenced by strain hardening. The model in Eq. (5) can accurately represent this strain hardening.

3.4. Creep strain curves

Before Eqs. (1) and (5) are used to predict creep strain curves, Eq. (8) must be transferred to effective stresses. This is done in the following way:

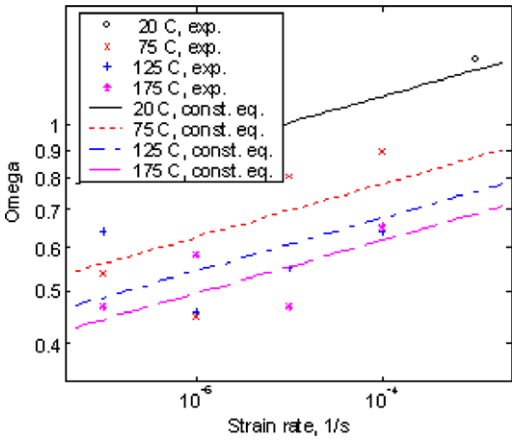

Fig. 3. The ω-values according to Eq. (12) versus strain rate are compared to the data that have been determined for each tensile test.

$$\frac{d\varepsilon_{cr}}{dt} = \left.\frac{d\varepsilon_{cr}}{dt}\right|_{min} g_{rate}, \tag{13}$$

where

$$g_{rate} = \left(\frac{\sigma_1}{\sigma_1 - \sigma_{i1}}\right)^N, \tag{14}$$

where σ_1 and σ_{i1} are the true applied stress and the back stress at a given strain ε_1 that is taken as $\varepsilon_1 = 0.20$. ε_1 is approximately the strain where the creep rate takes its minimum. Examples of modelled creep strain curves at 175 °C for an applied stress of 150 MPa are given in Fig. 5. Since only primary and secondary creep are taken into account only the first part of the creep curves can be modelled.

There is considerable scatter between the curves. There seems to be less scatter in the creep rate than in the initial plastic strain. The modelled creep rate also compares favourably with the experimental data. The typical variation between curves is that between Fig. 5(a) and (b). The maximum difference between the model and the experimental data in all analysed creep curves is a factor of 2 in creep strain. The creep specimens had to be reloaded regularly since the maximum strain of the creep machines was exceeded. This gives the uneven appearance of the curves. In the primary stage the creep rate is rapidly decreasing, which is well accounted for in the model. The model approximately follows:

$$\frac{d\varepsilon_{cr}}{dt} = F e^{-\delta\varepsilon},$$

Table 4
Data ranges

Data temperature range (°C)	Data stress range (MPa)	Data strain rate range (1/s)	Max model stress range (MPa[c])	Max model strain rate range (1/s[c])	Fig. no.
20–175	145–210	1×10^{-9}–1×10^{-3}	140–210	1×10^{-12}–1×10^{-3}	1a
200–400	40–160	5×10^{-10}–1×10^{-6}	40–140	1×10^{-12}–1×10^{-3}	1b
20–175	145–210	1×10^{-7}–1×10^{-3}	140–210	1×10^{-12}–1×10^{-3}	6

[c] Based on physical limits.

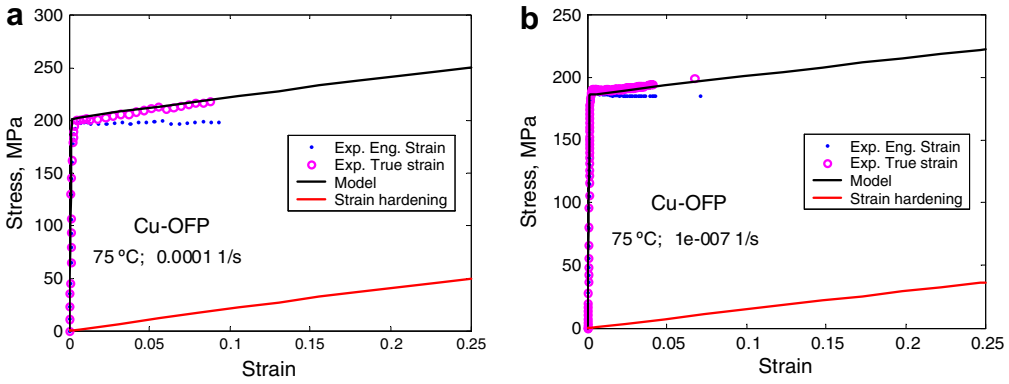

Fig. 4. Slow strain rate tensile curves. Experimental engineering and true stress are shown versus true strain as well as the model according to Eq. (11). The work hardening from Eq. (5) is shown separately. (a) 75 °C, 1×10^{-4} 1/s and (b) 75 °C, 1×10^{-7} 1/s.

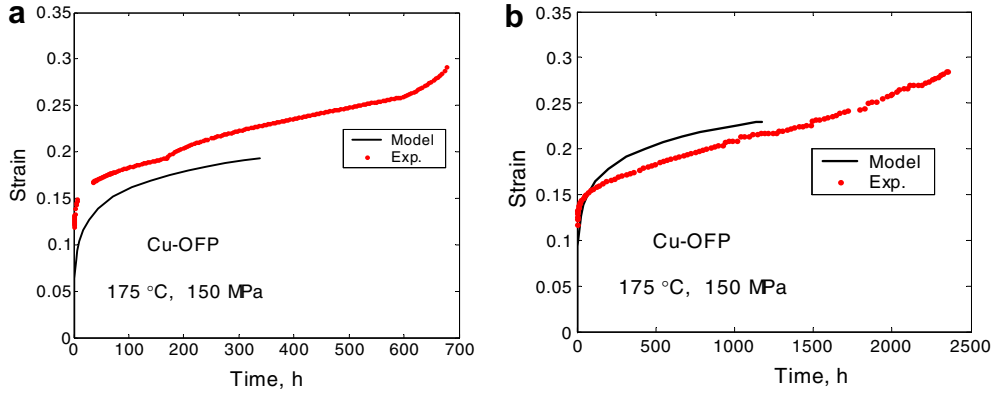

Fig. 5. Creep strain curves at 175 °C for a stress of 150 MPa. In (a) and (b) curves are tested under identical conditions.

where F and δ are constants. This behaviour is characteristic of the Ω-model [16–19].

3.5. Combined creep and stress–strain analysis

It has been illustrated above that both stress–strain and creep curves can be described by the presented model. The limitation is that different assumptions are made concerning the creep rate. In Section 3.3 the effective stress is applied directly in Eq. (8), since the stationary stress is equal to the effective stress in the tensile tests. However, in Section 3.4 for the creep curves the effective stress cannot be applied directly because the creep rate would be too low. Instead the correction in Eq. (13) for the back stress was introduced. Thus one must know in advance whether the application is strain rate or stress driven.

To avoid this dilemma the following approach can be used. Instead of the minimum creep rate, the initial primary creep rate can be considered. The latter creep rate is not influenced by the dislocation back stress. The procedure is illustrated in Fig. 6.

The creep rates at 175 °C are now above the SSR-data, whereas when the minimum creep rates were used, the creep rates were below, see Fig. 1. Ideally the initial creep rates and the SSR-rates at 175 °C should agree. One reason

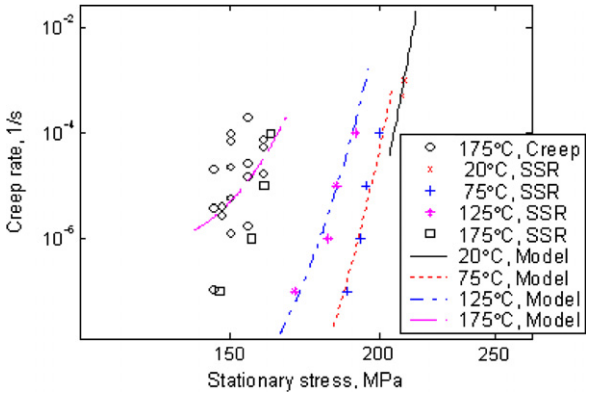

Fig. 6. Initial strain rate from creep tests and strain rate from SSR-tests as a function of stress. Data interval 20–175 °C.

that the SSR-rates are lower is that the copper used for the SSR-tests was cold worked whereas the creep tests were for annealed material. The variation of creep exponent is somewhat more pronounced than in Fig. 2. The origin of this effect is that the ratio between the initial and the minimum creep rates increases with decreasing stress. The constants used to fit the data in Fig. 6 are given in Table 3. The ranges for the applicability of the model are shown in Table 4. Neither the creep data nor the SSR-data in Fig. 6 are

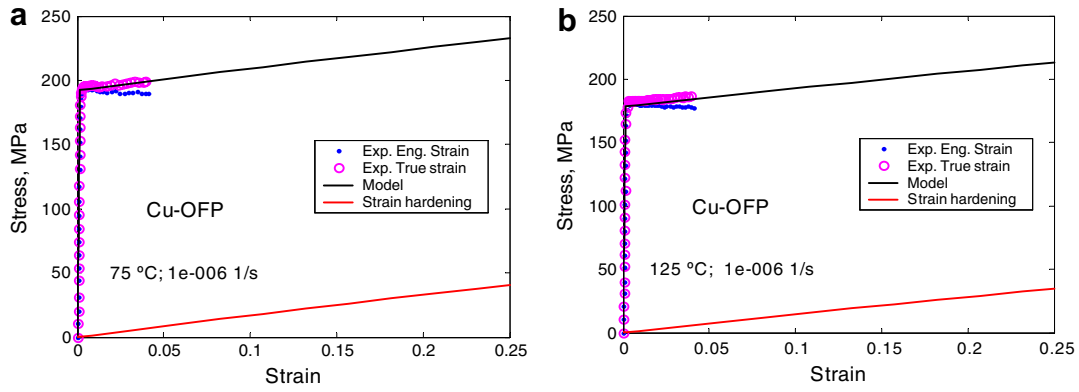

Fig. 7. Slow strain rate tensile curves. Experimental engineering and true stress are shown versus true strain as well as the model according to Eq. (9) with the constants in Table 3 (Fig. 6). The work hardening from Eq. (5) is shown separately. (a) 75 °C, 1×10^{-6} 1/s and (b) 125 °C, 1×10^{-6} 1/s.

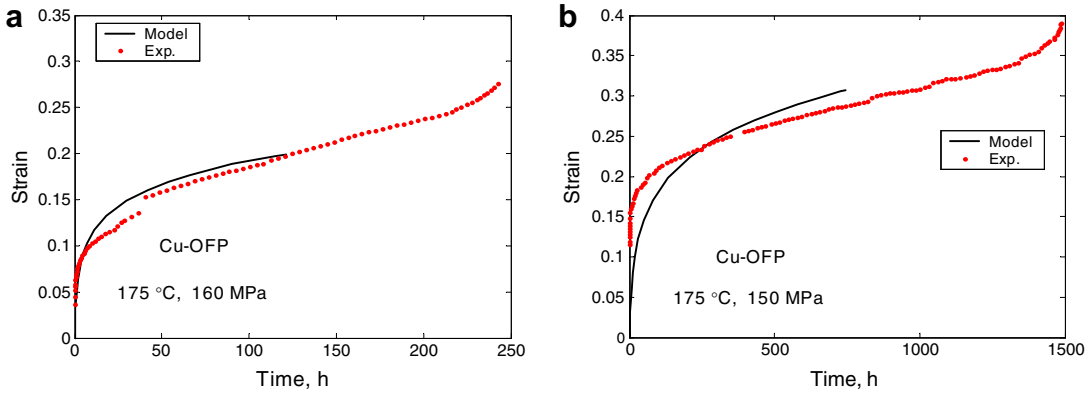

Fig. 8. Creep strain curves at 175 °C for different applied stresses modelled with Eq. (8) with constants in Table 3 (Fig. 6). (a) 160 MPa and (b) 150 MPa.

affected by the back stress. The consequence is that Eq. (8) can now be applied with the effective stress on the right hand side and without the correction in Eq. (13), Eq. (5) is valid as before.

To illustrate the use of the new approach, the constants in Table 3 (Fig. 6) are utilised to model stress–strain curves, see Fig. 7. As can be seen a good representation of the curves is obtained. The precision decreases somewhat with increasing temperature, primarily due to the large scatter at 175 °C.

Creep curves modelled with the combined approach are illustrated in Fig. 8. The same amount of variation between curves was observed as for those in Fig. 5.

The primary limitation of the combined approach is that it requires data covering the initial creep curves with good accuracy.

4. Basic creep model

4.1. Stationary stress

There has been much discussion in the literature about operating mechanisms during the deformation of pure fcc metals such as copper. In the high temperature regime above about half the melting point T_m the deformation is controlled by climb of dislocations. For copper $T_m/2 \approx 400$ °C. The climb rate of dislocations v_{climb} can be expressed as

$$v_{climb} = M_{climb} b \sigma, \tag{15}$$

where b is Burgers vector and M_{climb} the climb mobility. Hirth and Lothe gave the following expression for M_{climb} [20]:

$$M_{climb} = \frac{D_s b}{k_B T} e^{\frac{\sigma b^3}{k_B T}}, \tag{16}$$

where D_s is the self diffusion coefficient, k_B Boltzmann's constant and T the absolute temperature. The time dependent recovery of dislocation due to climb can be related to the climb mobility. This takes into account the annihilation of dislocation dipoles due to climb. Such a term can be added to Eq. (3)

$$\frac{d\rho}{d\varepsilon} = \frac{m}{bL} - 2\omega\rho - \frac{2}{\dot{\varepsilon}} M_{climb} \tau_L \rho^2, \tag{17}$$

where τ_L is the dislocation line tension. Ignoring the dynamic recovery term $2\omega\rho$ which is more important at lower

temperatures and considering stationary conditions, i.e. constant ρ, one finds that

$$\dot{\varepsilon} = \frac{2bc_L}{m}\frac{D_s b}{k_B T} e^{\frac{\alpha b^3}{k_B T}} \tau_L \rho^{3/2}. \quad (18)$$

In (18) it has again been assumed that L can be expressed as $c_L/\sqrt{\rho}$ where c_L is a constant. Inserting (4) into Eq. (18) shows that the creep rate behaves as σ^3, i.e. the Norton exponent is 3. The exponential term gives only a small effect. According to Eq. (18) the activation energy is the same as for the self diffusion coefficient. For pure copper Neumann et al. found an activation energy for self diffusion of 198 kJ/mol [21]. For creep, Raj and Langdon observed the value 180 kJ/mol at 500–600 °C [13]. All these basic facts that come out of Eq. (18) have been long established.

If we use Eq. (18), it gives approximately the correct creep rate for copper above 400 °C. If instead pipe diffusion is assumed to be dominating, Eq. (18) still gives a creep rate of the right order of magnitude from 400 down to 200 °C. The experimental creep exponent is, however far larger than 3 in this case, which makes the equation inapplicable. The selection of the pipe diffusion data for copper is explained in [22]. At still lower temperatures other mechanisms must enter as well. A common proposition is that the deformation is glide controlled [11]. Another one is that both low and high temperature deformation can be represented by a unified model [23]. We will combine these two approaches. Following [24] the glide of dislocations through an obstacle field may be written as

$$\frac{d\varepsilon}{dt} = f\sigma^2 e^{-\frac{Q}{RT}\left[1-\left(\frac{\sigma}{\sigma_{i\max}}\right)^{q_1}\right]^{q_2}}, \quad (19)$$

where Q is an activation energy, $\sigma_{i\max}$ the maximum back stress, and f, q_1 and q_2 constants. The constants q_1 and q_2 depend on the shape and distribution of obstacles to flow. $q_1 = 2$ and $q_2 = 1$ have been assumed in the present report, which are the same values as those chosen by Chandler [25]. When the applied stress approaches the tensile strength the recovery rate must be rapidly raised, otherwise the dislocation density would exceed its maximum possible value. This is sometimes referred to as spontaneous annihilation of dislocations [26]. The form of Eq. (19) can be seen as a generalisation of (18) and these two equations are combined in a unified model

$$\dot{\varepsilon}_{OF} = \frac{2bc_L}{m}\frac{D_{s0} b\tau_L}{k_B T}\left(\frac{\sigma}{\alpha m G b}\right)^3 e^{\frac{\alpha b^3}{k_B T}} e^{-\frac{Q_{eff}}{RT}\left[1-\left(\frac{\sigma}{\sigma_{i\max}}\right)^2\right]}. \quad (20)$$

In Eq. (20) the activation energies for climb and glide are given the same value. $\sigma_{i\max}$ should take a value just above the tensile strength $R_m \cdot \sigma_{i\max} = 1.2R_m$ has been chosen. All other parameters in Eq. (20) are readily available except c_L. Assuming the typical value for the initial work hardening rate of $G/200$ [15], c_L takes the value 57 according to Eqs. (3)–(5). Other constants used in Eq. (20) are given in Table 5.

Eq. (20) (for Cu-OF) is compared to experimental data in Fig. 9, where the creep rate is given versus the applied stress. The equation describes the general behaviour of data reasonably well. The difference between the model and the data is typically one order of magnitude or less.

The creep rate according to Eq. (20) is valid for pure copper. Next, the equation is going to be applied to copper alloyed with about 50 ppm phosphorus Cu-OFP. The creep rate in this alloy is essentially lower than in pure copper (Cu-OF). Experimental data for the ratio in creep rate between the two types of materials is shown in Fig. 10.

The following relation is used to describe the influence of phosphorus [22]:

$$f_P = \frac{\dot{\varepsilon}_{OF}}{\dot{\varepsilon}_{OFP}} = \begin{cases} K_1 \exp(K_2 e^{-k_3 T}) & T > 348\ \text{K} \\ K_0 & T \leqslant 348\ \text{K} \end{cases}, \quad (21)$$

where $K_0 = 3000$, $K_1 = 0.1695$, $K_2 = 55.73$ and $k_3 = 0.005\ 1/°C$ are constants. Combining Eqs. (20) and (21) gives an expression for the creep rate of Cu-OFP

$$\dot{\varepsilon}_{OFP} = \frac{2bc_L}{m}\frac{D_{s0} b\tau_L}{k_B T}\left(\frac{\sigma}{\alpha m G b}\right)^3 e^{\frac{\alpha b^3}{k_B T}} e^{-\frac{Q_{eff}}{RT}\left[1-\left(\frac{\sigma}{\sigma_{i\max}}\right)^2\right]} \Big/ f_P. \quad (22)$$

The use of Eq. (20) for Cu-OF was illustrated in Fig. 9. In the same way Eq. (22) is used in Fig. 11 to demonstrate the behaviour for Cu-OFP.

The same order of magnitude agreement to the data as for Cu-OF is observed. Naturally the representations in Figs. 9 and 11 are less precise than the fitted constitutive equations in Section 3 in the ranges of experimental data.

Table 5
Values of constants in Eq. (20)

Parameter description	Parameter	Value	Reference
Coefficient for self diffusion	D_{s0}	1.31×10^{-5} m^2/s	[21]
Activation energy for self diffusion	Q_s	198 000 J/mol	[21]
Burgers vector	b	2.56×10^{-10} m	
Strain hardening constant	c_L	57	
Taylor factor	m	3	
Boltzmann's constant	k_B	1.381×10^{-23} J/grad	
Constant in Eq. (4)	α	0.19	
Shear modulus	G	$G = 4.75 \times 10^4 - 17T$ MPa, T in K	[13]
Activation energy for creep at high temperatures	Q_{eff}	198 000 J/mol	[21]
Max back stress	$\sigma_{i\max}$	257 MPa	
Dislocation line tension	τ_L	7.94×10^{-16} MN	

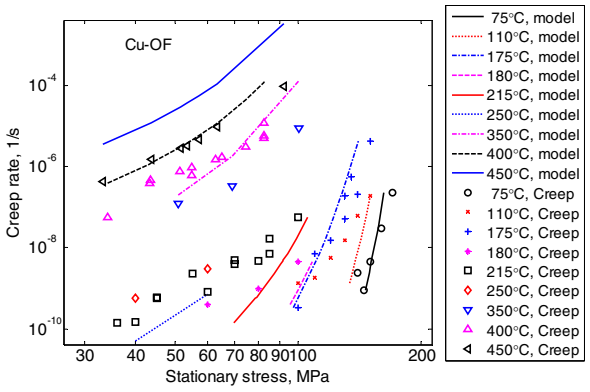

Fig. 9. Creep rate as a function of stress for Cu-OF. Model from Eq. (20). Data interval 75–450 °C. Data taken from [22] ($T < 300$ °C) and [13] ($T > 300$ °C).

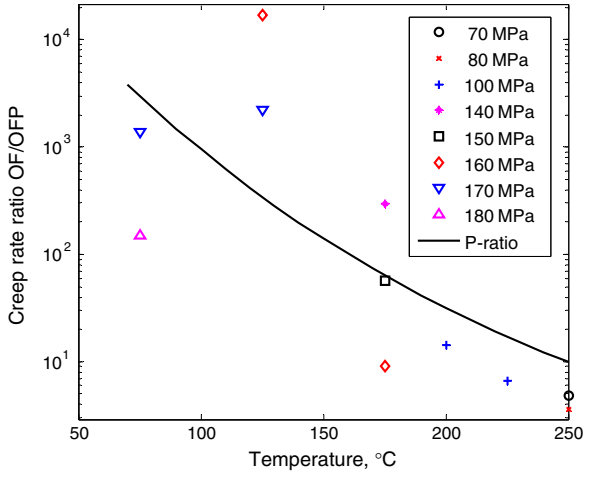

Fig. 10. The ratio in creep rate between Cu-OF and Cu-OFP versus temperature. The curve marked P-ratio is the empirical expression in Eq. (22).

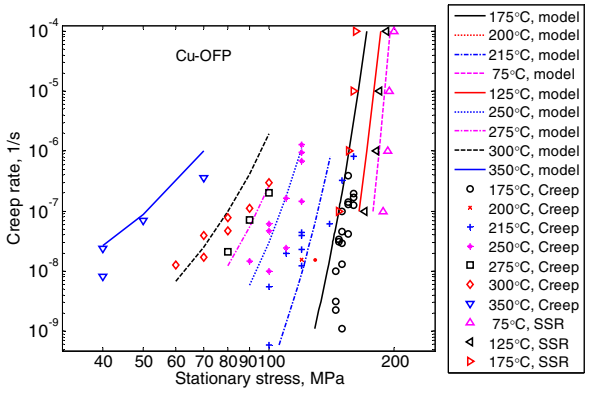

Fig. 11. Creep rate as a function of stress for Cu-OFP. Model from Eq. (20) also taking Eq. (21) into account. Data interval 75–350 °C.

However, due to the fundamental nature of Eq. (20) and to some extent of Eq. (21) [22], these equations are safer to use if extrapolation outside the experimental data ranges is needed.

Using the definition in Eq. (9), Eq. (20) gives the following expression for the creep exponent:

$$N = 3 + \frac{2Q_{\text{eff}}}{RT}\left(\frac{\sigma}{\sigma_{i\max}}\right)^2. \tag{23}$$

Eq. (23) is illustrated in Fig. 12 for Cu-OF and in Fig. 13 for Cu-OFP. N has a quadratic stress dependence.

In Fig. 13 a comparison is also made with the results in Fig. 2. The values from the fits in Fig. 2 are of the same order as those from Eq. (22). The comparison again illustrates that it would be risky to extrapolate the fitted constitutive equations.

An effective activation energy Q can be defined as

$$Q = RT\frac{\partial \log \dot{\varepsilon}_{\text{crmin}}}{\partial \log T}. \tag{24}$$

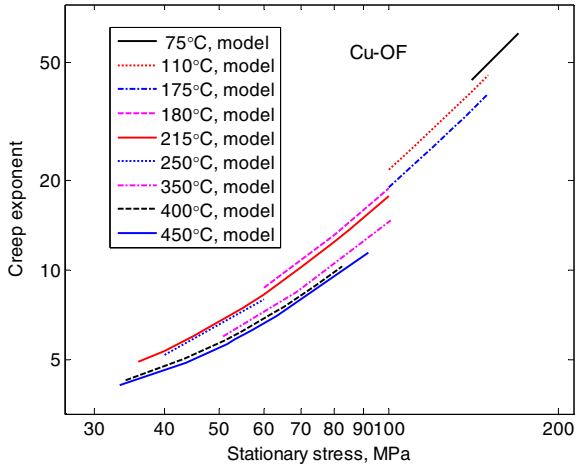

Fig. 12. Creep exponent versus stress. Model from Eq. (23). Data interval 20–400 °C.

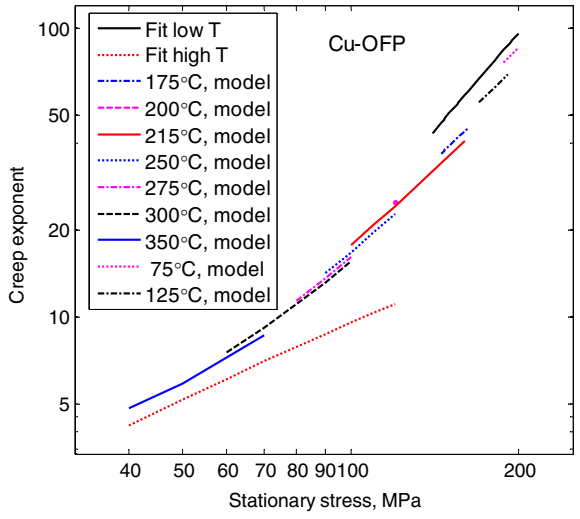

Fig. 13. Creep exponent versus stress. Model from Eq. (23). Data interval 20–400 °C. The curves marked Fit low T and Fit high T are taken from Fig. 2, respectively.

Applying this equation to Eq. (22) gives

$$Q = \left(Q_{\text{eff}} - \frac{\sigma b^3 R}{k_B}\right)\left[1 - \left(\frac{\sigma}{\sigma_{i\max}}\right)^2\right] + K_2 k_3 R T^2 \exp(-k_3 T). \quad (25)$$

In the first factor in Eq. (25), $Q_{\text{eff}} = 198$ kJ/mol is the activation energy for self diffusion in pure copper. The second term in the first factor $\sigma b^3 R/k_B$ takes values between 0.5 and 2 kJ/mol and is almost negligible in comparison to the first term. The temperature dependence in Eq. (21) has been taken into account and it appears as the last term in (25). Eq. (25) is illustrated in Fig. 14. The top curves represent Eq. (25) for Cu-OFP. The middle full drawn line is Eq. (25) with $K_2 = 0$, i.e. the case for Cu-OF. Below 100 MPa there is slow increase in Q with decreasing stress. This has also been observed by Raj and Langdon for Cu-OF [13] although the absolute values are slightly lower than in the present study, see Fig. 14. Above 100 MPa there is rapid decrease in the activation energy with increasing stress. The activation energy is considerably larger for Cu-OFP than for Cu-OF. The difference decreases somewhat with increasing temperature.

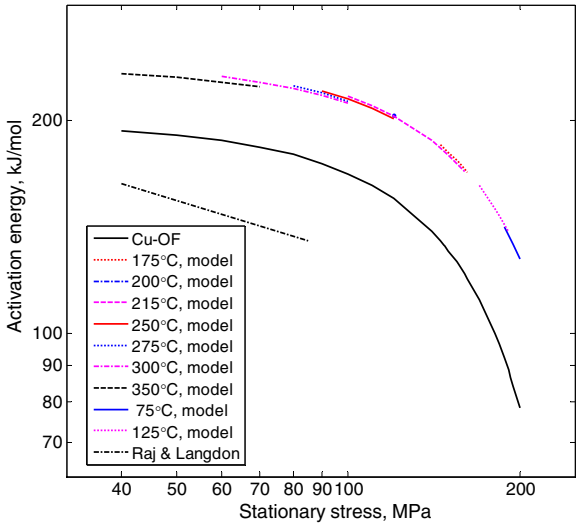

Fig. 14. Activation energy versus stress. The middle line: Eq. (25) for Cu-OF. Top lines: Eq. (25) for Cu-OFP. The bottom line: Cu-OF data from Raj and Langdon [13].

4.2. Use of effective stress in the basic creep model

Eq. (20) is based on the assumption that the full applied stress σ is used. In the modelling of general creep and stress–strain behaviour the effective stress σ_{eff} is the basis. In the same way as in Section 3.5, this change can be implemented by involving the initial creep rate rather than the minimum creep rate. This can be handled in the same way as in Eq. (13). An alternative way is to use the fact that an accurate representation of the primary creep strain can be obtained with the help of the ϕ-model [19]

$$\dot{\varepsilon} = \phi_1 \varepsilon_{\text{prim}}^{-\phi_2}, \quad (26)$$

$$\varepsilon_{\text{prim}} = (\phi_1(1+\phi_2)t)^{1/(1+\phi_2)}, \quad (27)$$

where $\varepsilon_{\text{prim}}$ is the primary creep strain, and ϕ_1 and ϕ_2 are constants. The use of the ϕ-model is illustrated in Fig. 15. The tertiary creep is handled with the Ω-model [17–19]

$$\frac{d\varepsilon}{dt} = \Omega_3 e^{\Omega_4 \varepsilon}, \quad (28)$$

where Ω_3 and Ω_4 are constants. No secondary creep is taken into account.

It has been found that many creep strain versus time curves for copper can be well represented in this way. The constants are determined by fitting to the data. The slope of the primary creep curves in Fig. 15 is controlled by the constant ϕ_2, see Eq. (27). The temperature and stress dependence of this constant is illustrated in Fig. 16.

As can seen from Fig. 16, ϕ_2 depends mainly on the temperature. This dependence is represented with the following linear relation:

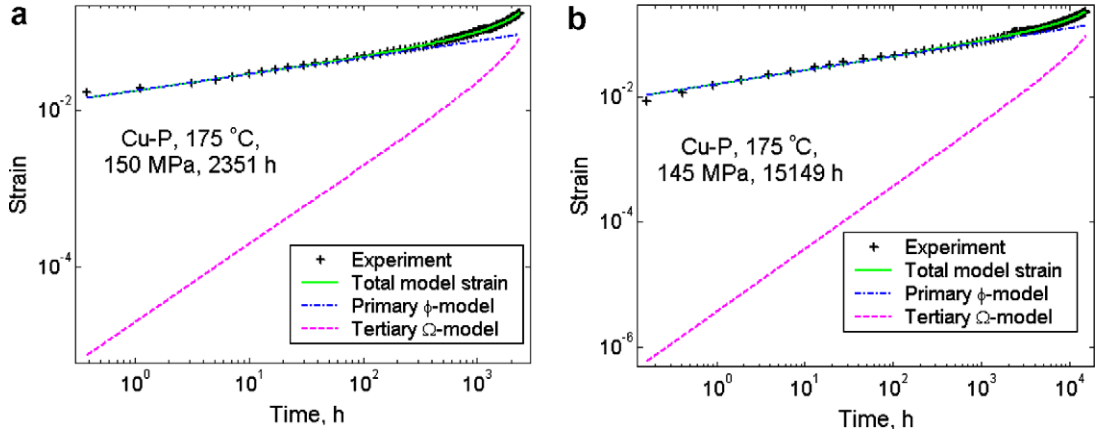

Fig. 15. Two creep curves for 150 and 145 MPa at 175 °C. The rupture times were 2351 and 15149 h. The primary creep is represented with the ϕ-model and the tertiary creep with the Ω-model.

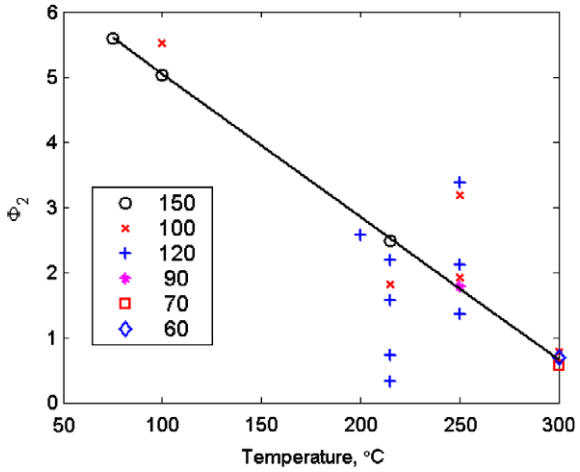

Fig. 16. Constant ϕ_2, in Eq. (27) versus temperature at stress levels from 60 to 150 MPa.

$$\phi_2 = 13.3 - 0.022T, \tag{29}$$

where the temperature T is given in Kelvin.

According to Eq. (26) the ratio between the initial creep rate $\dot{\varepsilon}_{\text{init}}$ and the minimum creep rate $\dot{\varepsilon}_{\text{min}}$ satisfies

$$\frac{\dot{\varepsilon}_{\text{init}}}{\dot{\varepsilon}_{\text{min}}} = \left(\frac{\varepsilon_{\text{init}}}{\varepsilon_{\text{min}}}\right)^{-\phi_2}. \tag{30}$$

If the ratio in Eq. (30) is combined with Eq. (20), the latter relation can be used with the effective stress. By analysing the data for creep curves it has been found that $\varepsilon_{\text{min}}/\varepsilon_{\text{init}} \sim 7.5$ can be used in Eq. (30) to obtain an estimate of the initial creep rate.

5. Multiaxial formulation of flow rule

A flow rule for elasto-plastic deformation with kinematic and isotropic hardening taken into account has frequently been used, for example by Chaboche and coworkers [27]. Back stress tensors are introduced to represent the kinematic hardening. The isotropic part is handled as a function of the equivalent plastic strain. Below a brief summary of the model is given. It is demonstrated below that the representation in Section 3 can be transferred to multiaxial stresses with this model.

The generalised Hooke's law for multiaxial stresses can be expressed as

$$\boldsymbol{\varepsilon}^{\text{e}} = \frac{1+\nu}{E(T)}\boldsymbol{\sigma} - \frac{\nu}{E(T)}Tr(\boldsymbol{\sigma}), \tag{31}$$

where $\boldsymbol{\varepsilon}^{\text{e}}$ is the elastic strain tensor, $\boldsymbol{\sigma}$ the stress tensor, ν Poisson's ratio, and $E(T)$ the temperature dependent elastic modulus. The total strain tensor increment can be written as

$$\mathrm{d}\boldsymbol{\varepsilon} = \mathrm{d}\boldsymbol{\varepsilon}^{\text{e}} + \mathrm{d}\boldsymbol{\varepsilon}^{\text{p}}, \tag{32}$$

where $\mathrm{d}\boldsymbol{\varepsilon}^{\text{e}}$ and $\mathrm{d}\boldsymbol{\varepsilon}^{\text{p}}$ are the elastic and the plastic strain tensor increment including the creep strain, respectively. Using (31) a relation can be obtained between the strain and stress increments

$$\mathrm{d}\boldsymbol{\sigma} = \mathbf{E}(\mathrm{d}\boldsymbol{\varepsilon} - \mathrm{d}\boldsymbol{\varepsilon}^{\text{p}}), \tag{33}$$

where $\mathbf{E}$ is the elastic stiffness tensor. Instead of using a plastic flow rule which is the traditional approach [27], a viscoplastic model can be utilised [28]. This is consistent with the presentation in Section 3. In its simplest form an effective strain rate is introduced in the following way:

$$\dot{p} = A\langle J(\boldsymbol{\sigma} - \boldsymbol{\sigma}_i) - \sigma_{y0} - K\rangle^n. \tag{34}$$

The brackets are defined by $\langle w\rangle = wH(w)$ where $H(w)$ is the Heaviside function ($H(w) = 0$ if $w < 0$, $H(w) = 1$ if $w \geqslant 0$). The constants A and n are the same as in Eq. (7). J is the second order stress invariant

$$J(\boldsymbol{\sigma} - \boldsymbol{\sigma}_i) = \sqrt{\frac{3}{2}(\boldsymbol{\sigma}' - \boldsymbol{\sigma}_i') : (\boldsymbol{\sigma}' - \boldsymbol{\sigma}_i')}, \tag{35}$$

$\boldsymbol{\sigma}'$and $\boldsymbol{\sigma}_i'$ are the deviatoric part of the stress and back stress tensor $\boldsymbol{\sigma}$ and $\boldsymbol{\sigma}_i$, respectively. : represents tensor multiplication element by element. $\sigma_{\text{y}} = \sigma_{y0} + K\left(\varepsilon_{\text{eff}}^{\text{p}}\right)$ is the isotropic yield function. In the present work the isotropic yield function is neglected. $\varepsilon_{\text{eff}}^{\text{p}}$ is the effective plastic strain. $\varepsilon_{\text{eff}}^{\text{p}}$ is given by

$$\mathrm{d}\varepsilon_{\text{eff}}^{\text{p}} = \sqrt{\frac{2}{3}\mathrm{d}\boldsymbol{\varepsilon}^{\text{p}} : \mathrm{d}\boldsymbol{\varepsilon}^{\text{p}}}. \tag{36}$$

With the help of (34) a viscoplastic strain rate is derived

$$\frac{\mathrm{d}\boldsymbol{\varepsilon}^{\text{p}}}{\mathrm{d}t} = \frac{3}{2}\dot{p}\frac{\boldsymbol{\sigma}' - \boldsymbol{\sigma}_i'}{J(\boldsymbol{\sigma} - \boldsymbol{\sigma}_i)}. \tag{37}$$

Eq. (37) has the same form as Odqvist's creep equation for multiaxial stress states but with a back stress tensor introduced. To describe the time dependence of the back stress tensor the Armstrong–Frederick non-linear law is used [29]

$$\frac{\mathrm{d}\boldsymbol{\sigma}_i}{\mathrm{d}t} = \frac{2}{3}a_{\text{k}}\frac{\mathrm{d}\boldsymbol{\varepsilon}^{\text{p}}}{\mathrm{d}t} - c_{\text{k}}\boldsymbol{\sigma}_i\frac{\mathrm{d}\varepsilon_{\text{eff}}^{\text{p}}}{\mathrm{d}t}, \tag{38}$$

where a_{k} and c_{k} are the kinematic hardening parameters. Eq. (38) is now expressed in terms of strain increments rather than in time increments

$$\frac{\mathrm{d}\boldsymbol{\sigma}_i}{\mathrm{d}\varepsilon_{\text{eff}}^{\text{p}}} = \frac{2}{3}a_{\text{k}}\frac{\mathrm{d}\boldsymbol{\varepsilon}^{\text{p}}}{\mathrm{d}\varepsilon_{\text{eff}}^{\text{p}}} - c_{\text{k}}\boldsymbol{\sigma}_i. \tag{39}$$

Comparing Eqs. (5) and (39) one finds that

$$c_{\text{k}} = \omega, \tag{40}$$

$$a_{\text{k}} = \omega C. \tag{41}$$

Eq. (34) can be generalised to correspond to Eq. (10)

$$\dot{p} = A\langle J(\boldsymbol{\sigma} - \boldsymbol{\sigma}_i) - \sigma_{y0} - K\rangle^{n(T)}\mathrm{e}^{\beta J(\boldsymbol{\sigma}-\boldsymbol{\sigma}_i)}\mathrm{e}^{-\frac{q(T)}{RT}}. \tag{42}$$

In this way a generalisation of Eqs. (5) and (10) to a multiaxial stress state has been established. In a similar way the basic model in Eq. (22) can be generalised to multiaxial stresses

$$\dot{p} = \frac{2bc}{m}\frac{D_{s0}b\tau_L}{k_B T}\left(\frac{J(\boldsymbol{\sigma}-\boldsymbol{\sigma}_i)}{\alpha m G b}\right)^3 \times e^{\frac{J(\boldsymbol{\sigma}-\boldsymbol{\sigma}_i)b^3}{k_B T}} e^{-\frac{Q_{eff}}{RT}\left[1-\left(\frac{J(\boldsymbol{\sigma}-\boldsymbol{\sigma}_i)}{\sigma_{imax}}\right)^2\right]} g_{rate} \Big/ f_P. \quad (43)$$

In Eq. (43), Eq. (14) has also been taken into account.

6. Discussion

Copper in the Swedish waste package canisters for used nuclear fuel will be exposed to creep at temperatures below 100 °C. Stresses of interest in this temperature range is inside the power-law breakdown regime. This can be illustrated in the following way. The absolute lowest creep rate that could affect the canister is 1% in 10^6 years, which corresponds to a rate of 3×10^{-16} s^{-1}. If Eq. (22) is used a stress of 105 MPa at 100 °C gives this rate. From Eq. (23) a creep exponent of 24 is obtained at this condition. At still lower temperatures and higher stresses the exponent would be higher than this value. It can be concluded that the range of technical interest is well inside the power-law breakdown regime.

When computing creep deformation in components during design two alternative approaches can be used. If the stresses in the component to be analysed do not vary much and the initial primary stage is not too important, expressions based on the stationary creep rate can be used. On the other hand if the stresses are strongly varying in the component an approach based on the effective stress should be applied. In this way the loading history of the component can be taken into account. The former situation will be referred to as the stationary case and the latter to as the non-stationary one. In the stationary case the creep rate can be related to the applied stress and expressions can be obtained directly from the experimental data. In the non-stationary case the back stress must be computed and the expressions in the stationary case must be translated to be applicable. It is obvious that if the stationary approach can be used one can expect a more accurate result since fewer computational steps are involved.

Norton type expressions for the creep rate as a function of the applied stress were derived by direct fitting to the experimental data, Eq. (7). Since there is a dramatic change of the creep behaviour in the interval around 175–200 °C, the data was split up in two temperature ranges. The resulting coefficients are given in Table 3. In the stationary case these expressions can be applied directly in design. Although reasonably accurate in the range of experimental data, these expressions are not suitable for extrapolation. In the temperature interval 20–175 °C experimental data are available from 140 to 210 MPa. In this temperature interval, Eq. (7) should thus not be used below 140 MPa.

To handle lower stresses an expression, Eq. (20) based on fundamental deformation principles for climb and glide has been derived. With this expression the observed creep rates of Cu-OF can be predicted within about an order of magnitude. Due to the basic nature of this expression and since it does not involve any fitted parameters, it is believed that it can be used more safely for extrapolation.

In [22] a fundamental relation for the ratio in creep rate between Cu-OF and Cu-OFP is derived. Unfortunately, this expression is not accurate enough to be used in design. Instead, a ratio is obtained by fitting a function to this data. This function is given in Eq. (21). Since extrapolation is not involved in this case, this function is the best available alternative.

In the non-stationary case the Kocks–Mecking model is used to compute the back stress. This has two important advantages. First, it is well known that this model can satisfactorily describe the plastic deformation of many fcc metals including copper. Second, there are established ways to translate the model to multiaxial stresses. The successful use of the model to describe the slow strain rate stress–strain curves demonstrates the validity of the Kocks–Mecking model.

New approaches are introduced to handle the transfer of stationary to non-stationary models. The basic principle is to base the models on the initial creep strain rate rather the minimum rate. At least for an annealed metal the initial back stress can be assumed to vanish. Then the same methods as for the stationary case can be applied but with minimum creep rate replaced by the initial one.

Two methods are used to relate the initial creep rate to the minimum one. According to the first method it is assumed that the typical strain where the creep rate is minimum is approximately known. The back stress at this strain is then computed and the initial rate can then directly be obtained. Comparisons to a number of experimental creep versus time curves verify this method.

In the second method it is assumed that the primary creep can be described by the ϕ-model. For individual creep curves this can be done with a very high precision. The intrinsic scatter between creep–time curves means that some approximations are involved when formulating a general model. This model is presented in Eq. (30). In principle this method is quite accurate but the difficulty lies in finding a precise value for the parameter ϕ_2.

In Section 5, an established model [27,28] is used to transfer the non-stationary uniaxial expressions to multiaxial stress states. It is demonstrated how the parameters in the multiaxial models are derived. In the stationary case there is no need to compute the back stress, so Eq. (38) can be ignored and the back stress can be assumed to vanish in the equations in Section 5.

7. Conclusions

- The creep properties of phosphorus alloyed copper (Cu-OFP) vary dramatically over the studied temperature interval between 20 and 400 °C. A generalised Norton model has been used to represent the temperature and

stress dependence of the minimum creep rate. The creep exponent takes values from 4 to 105 showing a pronounced power-law breakdown.

- A new unified model has been proposed to fully describe the transition from power-law to power-law breakdown. A fundamental expression for climb controlled creep has been combined with a model for glide controlled deformation. The new model gives creep rates of the right order of magnitude for the whole studied temperature range without the use of any fitted parameters.
- Computations of creep deformation in components can either be based on the applied stress or the effective stress. The former case is applicable when the stresses do not vary much in time. This is referred to as the stationary case. However, if the stresses have a pronounced time dependence the loading history must be considered. This is done with the help of the effective stress that is the difference between the applied stress and the back stress. The latter stress takes the loading history into account. This is referred as the non-stationary case.
- Ordinary creep strain data is in a form that can be directly used in the stationary case. To apply the data in the non-stationary case, two new methods have been developed. In both these methods the basic idea is to use the initial creep rate rather than the minimum value, which is the conventional way. In the first method the strain where the minimum creep rate occurs must be known. In the second method the ϕ-model is used to represent the primary creep which is possible with high precision.
- Constitutive equations for plastic deformation including creep have been formulated for Cu-OFP. The temperature range 20–400 °C has been covered. A generalised Norton model for the minimum creep rate has been combined with the Kocks–Mecking model for the back stress.
- The steady state creep rate, creep strain curves, and slow rate tensile stress–strain curves can be described adequately with the help of the constitutive equations.
- The derived constitutive equations have been generalised to multiaxial stress states to enable their use in finite element modelling.

Acknowledgments

The authors wish to thank the Swedish Nuclear Fuel and Waste Management Co. for funding this work.

References

[1] L. Werme, Design premises for canister for spent nuclear fuel, SKB, Stockholm, Technical Report TR-98-08, 1998. <www.skb.se>.
[2] P.J. Henderson, R. Sandström, Mater. Sci. Eng. A 246 (1998) 143.
[3] Technical Specification No KTS001 – Material for Copper Canisters, Swedish Nuclear Fuel and Waste Management Co (SKB), 1998.
[4] X.X. Yao, R. Sandström, Study of creep behaviour in P-doped copper with slow strain rate tensile tests, SKB TR-00-09, 2000. <www.skb.se>.
[5] J. Lindblom, P.J. Henderson, F. Seitisleam, Creep testing of oxygen-free copper and extrapolation of the results, Swedish Institute for Metals Research, Stockholm, Report IM-3197, 1995.
[6] F. Seitisleam, P.J. Henderson, J. Lindblom, Creep of copper for nuclear waste containment – results of creep and tensile tests on Cu-OF, Cu-OFP, cathode copper and welded joints, Swedish Institute for Metals Research, Stockholm, Report IM-3327, 1996.
[7] P.J. Henderson, L. Werme, Creep testing of copper for radwaste containers, Euromat 96 'Materials and Nuclear Power', Bournemouth, UK, October 1996.
[8] R. Sandström, J. Test. Eval. 27 (1) (1999) 31.
[9] H.C.M. Andersson, F. Seitisleam, R. Sandström, Influence of phosphorous and sulphur as well as grain size on creep in pure copper, Technical Report SKB TR-99-39, 1999. <www.skb.se>.
[10] H.C.M. Andersson, F. Seitisleam, R. Sandström, Creep testing of thick-wall copper electron beam and friction stir welds at 75, 125 and 175 °C, SKB, Stockholm, Technical Report TR-05-08. <www.skb.se>.
[11] H. Mecking, U.F. Kocks, Acta Metall. 29 (1981) 1865.
[12] R. Wu, R. Sandström, F. Seitesleam, J. Nucl. Mater. 336 (2–3) (2005) 279.
[13] S.V. Raj, T.G. Langdon, Acta Metall. 37 (1989) 843.
[14] Y. Estrin, H. Mecking, Acta Metall. 32 (1984) 57.
[15] U.F. Kocks, H. Mecking, Prog. Mater. Sci. 48 (2003) 171.
[16] R. Sandström, A. Kondyr, in: K.J. Miller, R.F. Smith (Eds.), Third International Conference on Mechanical Behaviour of Materials, Cambridge, vol. 2, Pergamon Press, Oxford, 1979, p. 275.
[17] R. Sandström, A. Kondyr, VGB Kraftwerkstechnik 62, Heft 9 (1982) 802–813 (in German).
[18] R. Wu, R. Sandström, J. Storesund, Mater. High Temp. 12 (1994) 277.
[19] R. Wu, R. Sandström, F. Seitesleam, J. Eng. Mater. Technol. 126 (2004) 87.
[20] J.P. Hirth, J. Lothe, Theory of Dislocations, McGraw-Hill, New York, 1968.
[21] G. Neumann, V. Tölle, C. Tuijn, Physica B: Condens. Matter 271 (1–4) (1999) 21.
[22] R. Sandström, H. Andersson, J. Nucl. Mater. 372 (1) (2008) 66.
[23] E. Nes, K. Marthinsen, Mater. Sci. Eng. A 322 (2002) 176.
[24] U.F. Kocks, A.S. Argon, M.F. Ashby, Prog. Mater. Sci. 19 (1975) 1.
[25] H.D. Chandler, Acta Metall. Mater. 42 (6) (1994) 2083.
[26] W. Blum, F. Roters, Phys. Status Solidi (a) 184 (1) (2001) 257.
[27] J.L. Chaboche, Int. J. Plast. 2 (2) (1986) 149.
[28] J.L. Chaboche, Int. J. Plast. 5 (3) (1989) 247.
[29] P.J. Armstrong, C.O. Frederick, A mathematical representation of the multiaxial Bauschinger effect, C.E.G.B. Report RD/B/N 731, 1966.